공학석사 학위논문

A Prediction of Clastic Reservoir Facies Using Hidden Markov Model Combined With Viterbi Algorithm

은닉마르코프모델과 비터비 알고리즘을 이용한

쇄설성퇴적암 저류층 암상 예측

2015 년 8 월

서울대학교 대학원

에너지시스템공학부

석 화 수

Abstract

A Prediction of Clastic Reservoir Facies Using Hidden Markov Model Combined With Viterbi Algorithm

Hwa-soo Suk

Department of Energy Systems Engineering

The Graduate School

Seoul National University

A facies of clastic rock affects reservoir properties such as permeability and porosity. A facies analysis in well is crucial to do a conditional facies modeling. Since a recovery of core cannot be performed through total depth due to the cost, the facies analysis is preferred to link well log data to stochastics methods.

Hidden Markov model (HMM) method, which predicts the facies from sedimentary -transition information and well log data, has been used for reservoir characterization. The conventional method is based on maximum a posteriori (MAP); selects a facies based on only maximum probability. This method performs poor with very thin layers

where probabilities are similar or input data are noisy.

In this study, Viterbi algorithm which can decrease uncertainty of decision and remove the meaningless thin layer, is included in HMM.

The proposed method is applied to the three clastic reservoir including two synthetic reservoirs and a shoreface reservoir. For C field in Louisiana, USA, it performed 12% better than conventional method and the transition-consistency ratio was increased by 70% for 18 wells.

Keywords: reservoir facies prediction, well log data, hidden Markov model, Viterbi algorithm.

Student Number: 2013-21017

Table of Contents

List of Tables

List of Figures

1. Introduction

A facies classification is one of the most important modeling components in reservoir characterization. A facies affects distributions of reservoir properties such as permeability and porosity. Reservoir facies are defined along the well path first. Then extend the facies classification to the entire reservoir. This process is called as conditional modeling **(Figure 1.1)**. A specific geological model of the facies strictly depends on the availability of core samples in the well. However, the recovery of cores is an expensive process and cannot be perform through the total depth. Obtaining core sample again for rehabilitative environment is difficult unlike well logs.

For these reasons, facies prediction should be integrated to well log data. Generally, facies are first defined based on core sample analysis combined with regional geological models volumes. Then log-facies are re-classified at the well location using well logs. If there is no core sample, we can estimate the facies after correlation analysis between core and well logs obtained from near wells **(Figure 1.2)**. In many application to reservoirs, log-facies classification relies on not only raw data of well logs also well log based petrophysical properties for example, porosity and mineralogical volume.

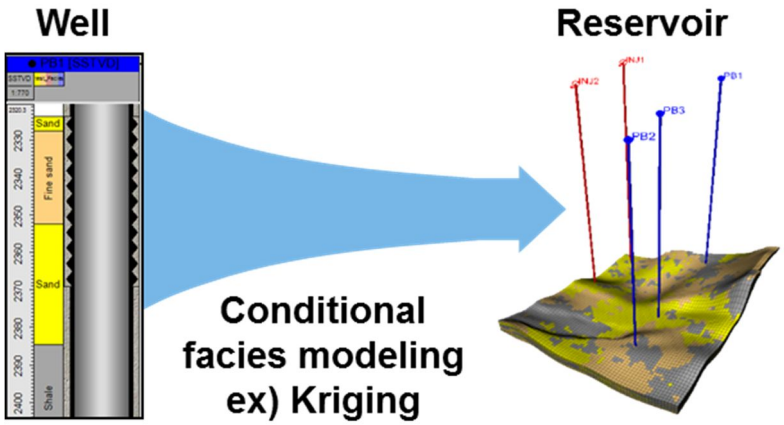

Figure 1.1 Conditional facies modeling for reservoir characterization.

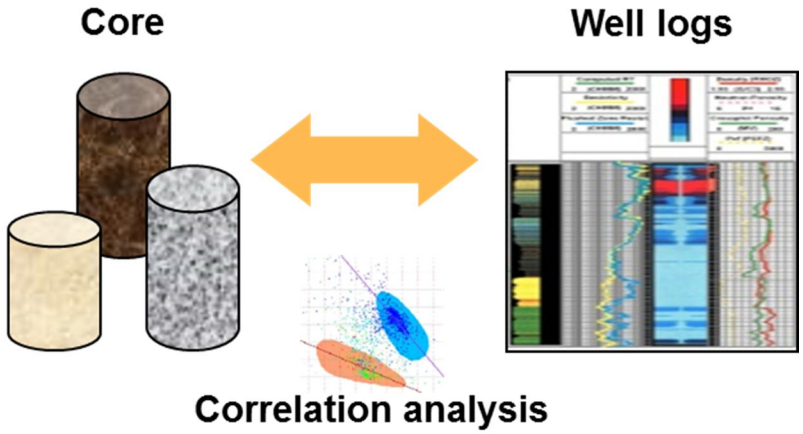

Figure 1.2 Correlation analysis between core and well logs.

The methods that have been used to classify facies using wireline logs can be generalized into two major categories:

(1) Deterministic methods, such as cut-off methods
(2) Statistical methods such as principal component analysis (PCA), fuzzy logic, and artificial neural network (ANN)

The deterministic methods, such as cut-off methods, are very simple. However, they are subjective and use limited number of well logs to discriminate. Gamma ray log can be used to discriminate sand and shale in a clastic reservoir based on 100 API. Using effective porosity curve and a cut-off value of 0.2 classify clean sand from shaly sand. However this method is not suitable in complex geological environments where multiple logs should be used to predict log-facies. When all the main well logs for instance neutron log, density log, gamma ray, and resistivity log or the computed petrophysical properties for example volumetric fractions are used simultaneously, deterministic methods are not adequate. There is a limitation on the number of well logs (Lindberg and Grana, 2015). For these reasons, statistical methods should be introduced. Since statistical method can suggest objective outputs, the results can be used for reference to beginners.

On the statistical approaches, Lim et al. (1997) used PCA and cluster analysis to classify facies from wireline logs with moderate success. Lee et al. (2004) and Mathisen et al. (2003) applied PCA, model based cluster analysis (MCA), and discriminant analysis (DA) to characterize electrofacies types and used nonparametric regression to predict permeability of a carbonate reservoir in west Texas. Jeong et al. (2013)

integrated the electrofacies characterization into fuzzy logic.

Lim and Kim (2004) reported using fuzzy logic and neural networks to delineate the nonlinear relationship between the best related well logs and reservoir properties. Wong et al. (1998) addressed important issues of improving neural-network performance such as outlier removal, data normalization and log calibration. Qi and Carr (2006) successfully used a back-propagation neural network to predict carbonate facies. Tang et al. (2011) used probabilistic neural network (PNN) to accurately predict facies from log data. Dubois et al. (2007) compared four approaches such as Bayes' rule, fuzzy logic, k-nearest neighbor, and ANN. The ANN clearly outperformed classification of rock type.

All these methods estimate the most likely facies classification at each location in the well log, but are difficult to account for the vertical continuity in the facies profile. Each sample in the well log is classified independently from the adjacent samples. Therefore unrealistic facies sequences could be created in the classified profile especially in sedimentary reservoir, for example very thin layers if the well logs are very noisy. Furthermore some transitions between facies could be more likely to happen than others, and other transitions could be unfeasible. An example can be described in shoreface reservoir. The shorefaces reservoir can be divided into upper shoreface facies (USF), middle shoreface facies (MSF), lower shoreface facies (LSF) and non-shoreface facies (NSF) (Walker and Print, 1992). Classification methods based on sample-by-sample classification could lead to unrealistic classifications, for example a MSF sample showed out deeper than LSF which is not physically possible without event of reversal

phenomenon. If vertical continuity is accounted for, these classification problems cannot be observed because of the constraints on geological transitions and layer thickness.

To improve the available prediction methods and include the vertical correlation in the facies profile, Markov models are applied. In order to apply Markov models, certain conditions need to be met as follows.

(1) The probability distribution of the next state depends on the current state in the space.
(2) The changes of state of the system are called transitions. These transitions have regularity or tendency.

If the states cannot be observed directly (it is hidden), but the output, dependent on the state, is visible, hidden Markov model (HMM) can be used for find the hidden states. Since a facies distribution depends on sedimentary environment and facies is related with adjacent facies type, Markov models can be adjusted in geological system. In the reservoir, it is difficult to know facies type, but information on the facies type alternations can be obtained indirectly from well logs measurement made along the length of drilled wells. For these reasons, using HMM for facies prediction is possible.

The use of Markov chains to model geological layering was first proposed by Krumbein and Dacey (1969), see also Elfeki and Dekking (2001) for an overview. Godfrey et al. (1970), Velzeboer (1981) and Sinvhal et al. used Markov chains to study the seismic response of layered stratigraphy.

Several applications of HMM exist in computer science, speech recognition, signal theory and biology, see for example Um (2001) for an overview. Eidsvik et al.

(2004) proposed the use of HMM for well log inversion into geological attributes in the same context as considered in this work, and estimated the parameters in a fully Bayesian framework requiring Markov chain Monte Carlo (McMC) calculations. Lindberg and Grana (2015) chose Expectation-Maximization algorithm (EM algorithm) known as Baum-Welch algorithm (Baum et al., 1970; Wu, 1983) to estimate the HMM parameters. The conventional HMM methods including HMM combined with McMC and EM were focused on optimization of HMM parameters.

The limitation of previous studies related with HMM is as follows. Conventional HMM methods determined facies based on maximum a posteriori (MAP); selects a facies based on only maximum probability. It could give improper results where probabilities are similar or data is noisy because it could not reflect the uncertainty of determination.

The objectives of this study are, first, guarantee vertical correlation in facies sequence for reservoir characterization. Second, improve prediction accuracy applying Viterbi algorithm included in HMM. Finally proposed method to target field with optimal log set.

This paper is composed of five chapters. Chapter 1 describes motivation of the studies, the research trends how to predict the facies and limitations of their works. Chapter 2 explains theoretical backgrounds in HMM, Viterbi algorithm and two parameters. In chapter 3, the methodology is proposed to facies prediction using HMM combined with Viterbi algorithm. Chapter 4 presents results of three different clastic

reservoirs and comparison with conventional method. Chapter 5 summarizes and concludes the thesis.

2. Theoretical Backgrounds

2.1. HMM (hidden Markov model)

The HMM is a doubly stochastic process with an underlying stochastic process that is not observable (it is hidden), but can only be observed through another set of stochastic processes that produce the sequence of observed symbols (Rabiner and Juang, 1986; Rabiner, 1989).

Markov properties have been recognized in many geological phenomena, including stratigraphic sequences of lithologic units, sedimentary process, stream drainage networks, succession of mineral occurrences in igneous rocks, sequence of volcanic eruptions, crystallographic disorder in carbonate crystals, etc (Krumbein and Dacey, 1969).

Geological observations can be structured as Markov chains (Krumbein and Dacey, 1969). The unknown facies profile can be represented as a sequence of unknown states of a process. A stochastic process has the (first-order) Markov property if the conditional probability distribution of future states of the process depends only upon the present state, not on the sequence of events that preceded it. A discrete-time stochastic process satisfying the Markov property is known as a Markov chain. A Markov chain is a sequence of random variables $\{Q_t\}_{t=1,\dots,T}$ with the Markov property, for any $1 < t \leq T$.

$$p(Q_{t+1} = q | Q_1 = q_1, \dots, Q_t = q_t) = p(Q_{t+1} = x | Q_t = x_t) \tag{2.1}$$

In this work, categorical Markov processes with a discrete-valued state space only are considered, therefore each state Q_t belongs to one out of N classes, for example for N possible facies classes. The probability on the right hand side of Eq. (2.1) is called the transition probability, which is assumed to be stationary throughout the sequence which is independent of t. These transition probabilities can be collected in a $(N \times N)$ matrix P, called the transition matrix. Define the probability of a transition from state i to state j as P_{ij}, then the transition matrix can be written as below (Eq. (2.2)).

$$\mathrm{P} = \begin{pmatrix} P_{11} & \cdots & P_{1n} \\ \vdots & P_{ij} & \vdots \\ P_{n1} & \cdots & P_{nn} \end{pmatrix} \tag{2.2}$$

Since there are only N possible states, the sum of transition probabilities from state i to the other states $j = 1, \cdots, N$ must be 1, that is each row of the matrix sums to 1 ($\sum_{j=1}^{N} P_{ij} = 1$).

$$sand \quad shale \quad limestone \tag{2.3}$$

$$P = \begin{pmatrix} 0.95 & 0.03 & 0.02 \\ 0.04 & 0.95 & 0.01 \\ 0 & 0.05 & 0.95 \end{pmatrix} \begin{matrix} sand \\ shale \\ limestone \end{matrix}$$

Rows correspond to sand, shale, and limestone at depth t, and columns refer to sand, shale, and limestone at depth $t + 1$ (downward transition) (Eq. (2.3)). The matrix is read (by row) as follows: if one knows that at depth t the actual facies is sand, then at depth $t + 1$ the probability of finding sand is 0.95, the probability of finding shale is 0.03, and the probability of finding limestone is 0.02. Similarly for the other rows. In the example the transition from sand to limestone is impossible (probability equal 0). Impossible transitions can be often found in transition probabilities of litho-fluid classes. A diagonal of the transition matrix have high probability means few facies transitions; a facies has a transition to itself. Zero-probabilities in the estimated transition matrix can happen due to the lack of transitions in the reference facies. However, to achieve a higher resolution classification and to achieve a more flexible model, all the entries in the transition matrix set to be non-zero because geologically none of these transitions are impossible. With unknown stratigraphic profile, a minimum probability of 0.01 is similarly set in each entry (Lindberg and Grana, 2015) so that transition matrix will be change from Eq. (2.3) to Eq. (2.4).

$$\begin{matrix} sand & shale & limestone \end{matrix} \tag{2.4}$$

$$P_{adj} = \begin{pmatrix} 0.95 & 0.03 & 0.02 \\ 0.04 & 0.95 & 0.01 \\ 0.01 & 0.05 & 0.94 \end{pmatrix} \begin{matrix} sand \\ shale \\ limestone \end{matrix}$$

A HMM is a model which is assumed to follow a Markov process with unobserved (hidden) states. Generally the Markov process itself cannot be observed (in other words the states cannot be measured) but indirect observations, related to the states, are available. For example, facies cannot be measured in the subsurface, but rock properties that depend on the facies type can be measured, such as porosity. Let the random variable O_t be the observation at time t, which relate to the corresponding hidden state at time t, O_t, is given by the probability density function (pdf) of O_t conditioned on Q_t, p($O_t|Q_t$), denoted the output probabilities.

The steps of facies prediction using different methods are displayed in **Figure 2.1**. Conventional methods without vertical dependency including ANN uses only well log data for input to predict facies at same depth **(Figure 2.1 (a))**. Whereas, HMM methods use not only well log data also adjacent facies information for input of model **(Figure 2.1 (b))**.

The complete set of HMM parameters for a given model by is described by $\lambda = \{\Pi, A, B\}$ where Π is the vector of global proportions of the facies which carry out transition probability at starting depth, A represents the facies transition matrix and B represents the parameters of the output probabilities of well log. These parameters can be easily estimated for example for the transition probabilities by counting the number

of transitions throughout the facies classification and normalization. **Table 2.1** summarizes HMM variables in this work.

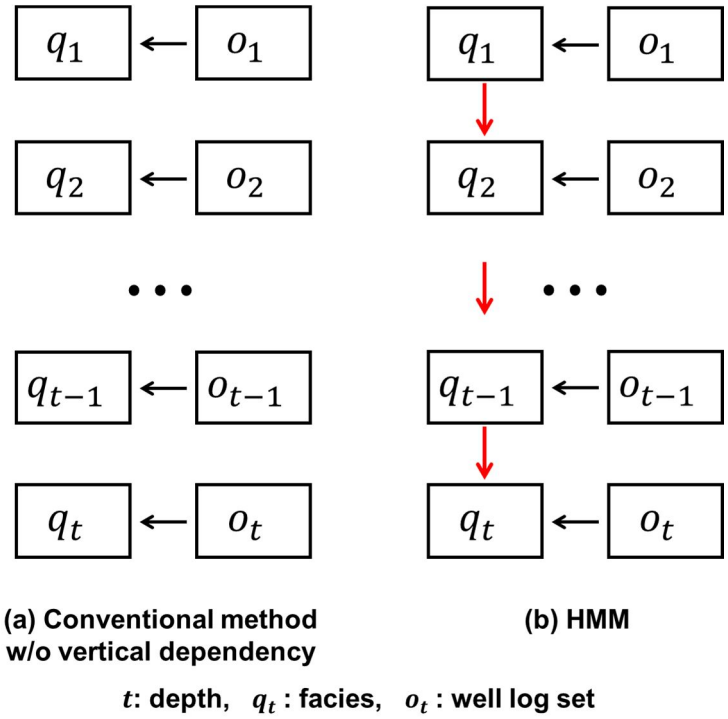

Figure 2.1 Step of facies prediction in conventional method without vertical dependency and HMM.

(Modified from Lindberg and Grana, 2015)

Table 2.1 Meaning of the HMM variables in this work.

HMM	Variable	This work
Hidden state set	$Q = \{q_1, \cdots, q_{t-1}, q_t\}$	Facies
Observable state sequence	$O = \{o_1, \cdots, o_{t-1}, o_t\}$	Well log sequence
π vector	Π	Global proportions of the facies
State transition matrix	$P = \begin{pmatrix} P_{11} & \cdots & P_{1n} \\ \vdots & P_{ij} & \vdots \\ P_{n1} & \cdots & P_{nn} \end{pmatrix}$	Facies transition probabilities
Observation probability matrix	$P(O\|Q)$	Well log pdf conditioned on facies
Length of the observable state sequence	$T = \{1, \cdots, t-1, t\}$	Depth
Number of states	$N = \{1, \cdots, n-1, n\}$	Number of facies

2.2. Viterbi algorithm

2.2.1 HMM issues

HMM discussed in the previous section, there are three key issues of interest for use the model. These issues are the following:

(1) Given the observation sequence $O = O_1, O_2, \cdots, O_T$ and the model $\lambda = \{\Pi, A, B\}$, how we compute $Pr(O|\lambda)$, the probability of the observation sequence.

(2) How we adjust the model parameters $\lambda = \{\Pi, A, B\}$ to maximize $Pr(O|\lambda)$.

(3) Given the observation sequence $O = O_1, O_2, \cdots, O_T$, how we choose a state sequence $I = i_1, i_2, \cdots, i_T$, which is optimal in some meaningful sense.

The first issue is the evaluation problem. We wish to calculate the probability of the observation sequence O, given the model λ. Forward algorithm and Backward algorithm are the most widely used method to compute the probability. The second issues is the parameter estimation problem. We attempt to optimize the model parameters such as global proportions, transition probabilities and output probabilities. To solve this issues, an iterative procedure such as EM algorithm or gradient techniques for optimization must be used. The third issues is optimal sequence problem. We want to determine the optimal state sequence as best as possible. There are several method to find it including Viterbi algorithm.

2.2.2 Viterbi algorithm

The Viterbi algorithm is a dynamic programming algorithm for finding the most likely sequence of hidden states – called the Viterbi path – that results in a sequence of observed events, especially in the context of Markov information sources and HMM (Viterbi, 1967; David, 1973; Lou, 1995).

There are several possible ways of solving the third issue. One possible optimality criterion is to choose the states which are individually most likely. However, there might be some problems with the above criterion and solution. Where there are disallowed state sequence may in fact be an impossible states sequence, or there are similar probabilities. By adding to transition information, it would prevent that problems. That's why the Viterbi algorithm can be one of the solution on the third issues.

The point of the Viterbi algorithm is that the algorithm postpone the determination. In other words, it doesn't determine one of the state at t and calculate the posterior probabilities at $t+1$. Finding the path to make the maximum of posterior probability at depth $t+1$ then select the one of states at t based on the path **(Figure 2.2)**.

The Viterbi algorithm is demonstrated on **Figure 2.3**. $\delta_t(j)$ is the probability of the most probable state sequence responsible for the first t observation that has j as its final state. The Viterbi path can be retrieved by saving back pointers that remember which state $\Psi_t(j)$. The step2, recursion process, is the mainly different with MAP.

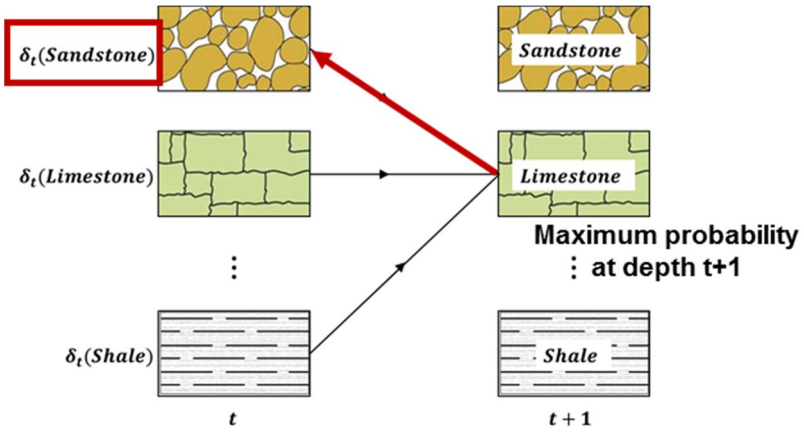

Figure 2.2 Principle of Viterbi algorithm at t and t+1.

- Step1: Initialization
  $\delta_1(i) = \pi_i b_i(o_q), 1 \leq i \leq N$
  $\Psi_1(i) = 0$

- Step2: Recursion
  For $2 \leq t \leq T, 1 \leq j \leq N$
  $\delta_t(j) = max[\delta_{t-1}(i)a_{ij}]b_j(o_t)$
  $\Psi_t(j) = argmax[\delta_{t-1}(i)a_{ij}]$

- Step3: Termination
  $P^* = \max[\delta_T(j)]$
  ${q_T}^* = argmax\ [\delta_T(i)]$

- Step4: Path (state sequence) backtracking
  For $t = T-1, T-2, \ldots, 1$
  ${q_t}^* = \Psi_{t+1}({q_{t+1}}^*)$

Figure 2.3 Viterbi algorithm (Rabiner and Jaung, 1986)

2.3. Consistency ratio parameters

A predictive performance is evaluated by the two parameters. $C1$ is called as facies-consistency ratio is general parameter to show successful facies prediction at each depth. $C2$ is called as transition-consistency ratio checks facies-transion frequency. $C2$ is possible to represent vertical spatial distributions. $C1$ and $C2$ are defined below equations for 0 to 1. Two parameters are modified from Lindberg et al. (2014, 2015) and they called as location-wise mismatch, mismatch on total number of transitions between different facies layers respectively (Eq. (2.5), Eq. (2.6)).

$$C1 = \frac{1}{T}\sum_{t=1}^{T} I(\hat{q}_t = q_t) \tag{2.5}$$

$$C2 = 1 - \frac{1}{\Delta\rho_{max}}|\rho(\hat{q}) - \rho(q)| \tag{2.6}$$

Where $\hat{Q} = \{\hat{q_1}, \cdots, \hat{q_t}\}$ is reference facies sequence, $Q = \{q_1, \cdots, q_t\}$ is predicted facies sequence, $T = \{1, \cdots, t\}$ is length of facies sequence, $\rho(\hat{q})$ is the number of reference layer transitions, $\rho(q)$ is number of predicted layer transition, $\Delta\rho_{max}$ is the number of probable maximum difference. $C2$ is very sensitive by $\Delta\rho_{max}$. If predicted facies sequence shows that facies are changed in every sample in other words $\rho(q)$ is T-1, but the transition frequency is a few, $\Delta\rho_{max}$ will be very high. However, it is impossible to happen with proper statistical method. Lindberg and Grana mentioned $C2$

has upper limits by setting $\Delta\rho_{max}$. $C2$ is redefined as Eq. (2.7). $\Delta\rho_{max}$ will be changed by reservoir.

$$C2 = 1 - \frac{1}{\Delta\rho_{max}} \min\{\Delta\rho_{max}, |\rho(\hat{q}) - \rho(q)|\} \tag{2.7}$$

Both $C1$ and $C2$ are close to 1 means successful facies prediction **(Figure 2.4)**. Using $C2$ with $C1$ is recommended for evaluate than only using $C2$. Characteristics of the plane is as below. **Figure 2.5** shows difference of each plan with reference.

1) Left side: predicted facies sequence mismatch with reference.
2) Right side: predicted facies sequence is similar with reference.
3) Upper side: predicted facies-transition frequency is similar with reference.
4) Lower side: predicted facies-transition frequency mismatch with reference.

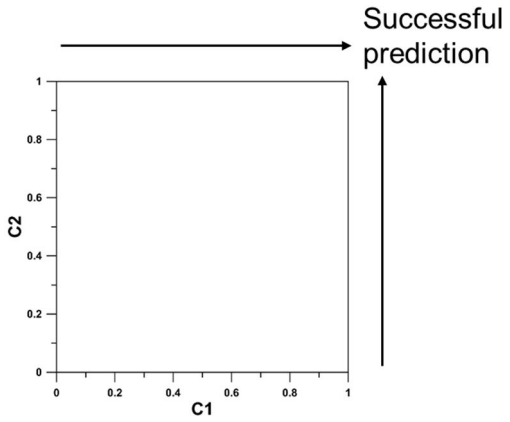

Figure 2.4 Successful prediction in 2D plot of $C1$ and $C2$.

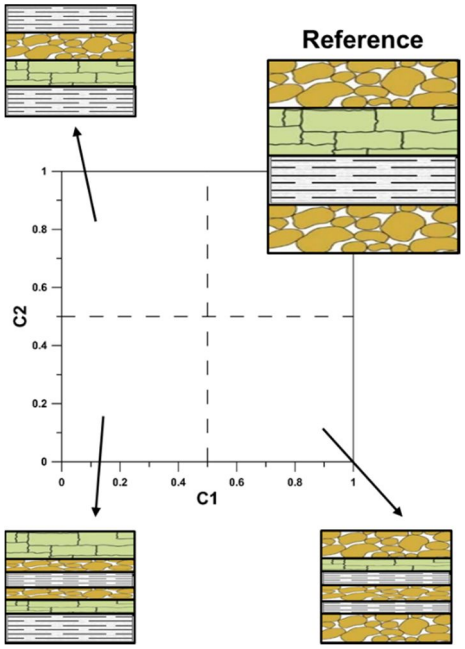

Figure 2.5. Tendency of facies profile based on 2D plot of $C1$ and $C2$.

3. HMM Method Combined with Viterbi Algorithm

Figure 3.1 summarizes steps focused on determination method of two methods. MAP selects one facies without next depth $t+1$ facies type. Viterbi algorithm reflects the deeper facies type. It can modify determination as adjacent facies

Figure 3.2 shows the procedures for conventional method. This method perform EM algorithm and it select one facies based on MAP after calculate the probabilities at the each depth (HMM-EM-MAP).

Figure 3.3 illustrates the procedures for the proposed method (HMM-EM-Viterbi). The first step of the proposed method is to get raw data such as well log and core data. Then perform several pre-processing to the data. For example, outlier removal for decreasing noise, normalization as shown in Eq. (3.1) and discretization of well log data.

$$X' = \frac{X - X_{min}}{X_{max} - X_{min}} \tag{3.1}$$

Next step is to make HMM by calculation of HMM parameters such as global facies-proportion, Π, used for transition probability at start depth, facies-transition probability, A, output of well log probability, B, depending on facies. In this studies the facies prediction proceed downward. A minimum probability of 0.01 is similarly set in each entry before running the EM algorithm.

Optimize the three parameters using EM algorithm. Estimates posterior probabilities using the Forward and Backward algorithms.

The last step of the proposed method is to predict facies sequence in target well with the Viterbi algorithm, which can remove the uncertainty of facies decision.

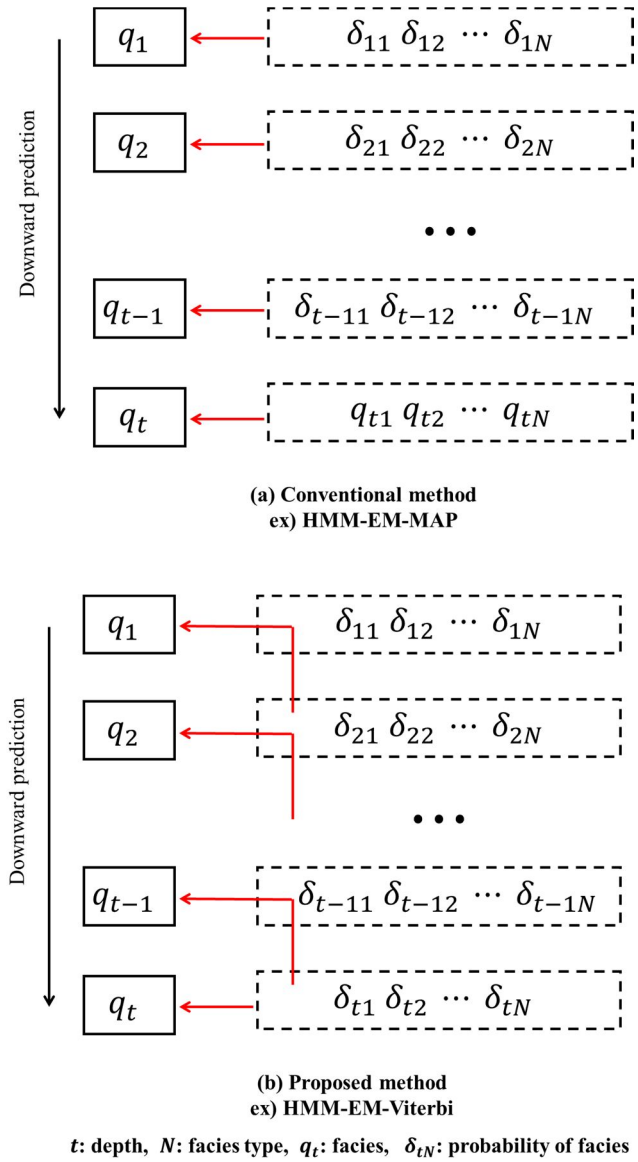

Figure 3.1 Step of facies prediction on MAP and Viterbi algorithm.

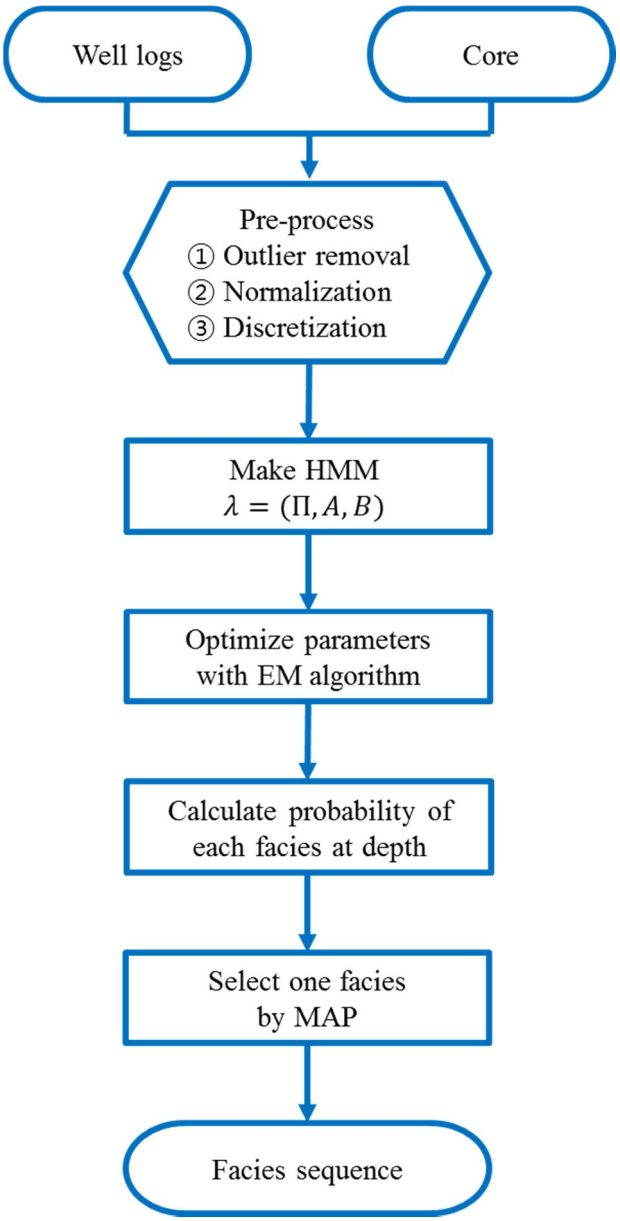

Figure 3.2. Flow chart of the conventional method.

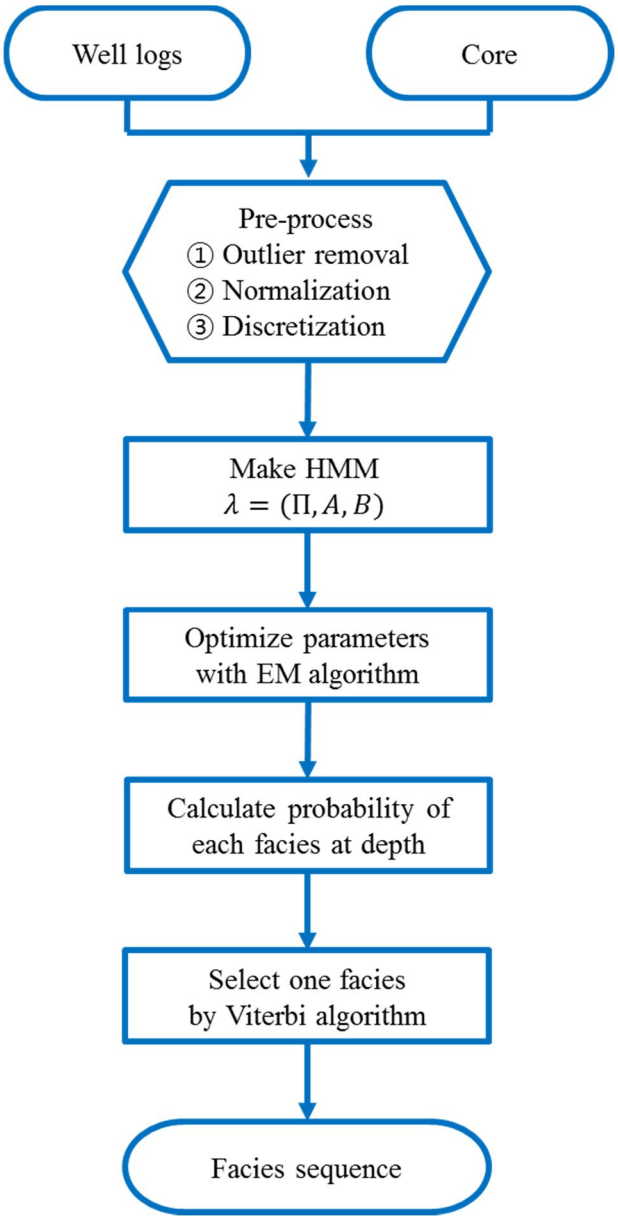

Figure 3.3. Flow chart of the proposed method.

4. Results and Discussion

4.1. Application to synthetic reservoir 'A' with four lithofacies

4.1.1 General description

The proposed method is applied to synthetic reservoir, A field, which is clastic reservoir. This field is consist of four different lithofacies such as sandstone, shaly sandstone, sandy sandstone and shale. **Table 4.1** shows the number of sample for each facies. **Table 4.2, Table 4.3, Table 4.4, Table 4.5 and Table 4.6** represent reservoir properties. Porosity, permeability and water saturation are obtained from core analysis. The others, clay volume and limestone volume, are calculated based on well logs.

There are common well logs and petrophysical properties computed from well logs. For example, gamma ray (GR), corrected gamma ray for wellbore size (GRC), normalized corrected gamma ray (GRN), shale base-line shifted spontaneous potential (SPBL), deep resistivity (ILD), medium resistivity (ILM), invasion corrected resistivity (RT), density porosity (DPHI), neutron porosity (NPHI), neutron and density total porosity (PHIND), modified Simandoux water saturation (SWQ), effective porosity (PHIEQ), clay volume (VCL), limestone volume (VLM). For these well logs, step size of data is 1ft.

Among them, ten of well log are selected for facies prediction in order to remove unwilled redundancy effect. The selective ten are GR, SPBL, RT, DPHI, NPHI, PHIND, SWQ, PHIEQ, VCL and VLM. It was selected based on correlation coefficient. Eq. (4.1)

shows how to calculate correlation coefficient. **Table 4.7** and **Table 4.8** show correlation coefficient for gamma ray logs and resistivity logs. Two-dimensional plots of 95% confidence regions (ellipse) for each facies is also good indicator for find similar log. The ellipse parallel to y=x means that the two loggings are highly correlated. The blue ellipse, pink ellipse, green ellipse, and red ellipse shows the tendency of sand, shaly sand, sandy shale, and shale respectively. The relevance between GR and GRC is high as shown in **Figure 4.1(a)**. ILD and RT are also highly correlated as shown in **Figure 4.1(b)**.

$$Corr(u,v) = \frac{1}{n-1}\sum_{i=1}^{n}\left(\frac{u_i - \bar{u}}{s_u}\right)\left(\frac{v_i - \bar{v}}{s_v}\right) \tag{4.1}$$

where

u, v : variables.

$\bar{u}, \bar{v}$: average.

s_u, s_v : standard deviation.

Table 4.1 Number of sample in A field

Facies	Sample size	Total
Sandstone	152	519
Shaly sand	218	
Sandy shale	119	
Shale	30	

Table 4.2 Porosity of A field

Facies	Porosity, dec			
	Avg.	Std.	Min	Max
Sandstone	0.20	0.04	0.04	0.23
Shaly sand	0.20	0.04	0.05	0.28
Sandy shale	0.18	0.05	0.04	0.23
Shale	0.12	0.05	0.06	0.20

Table 4.3 Permeability of A field

Facies	Permeability, md			
	Avg.	Std.	Min	Max
Sandstone	48.63	42.27	0	197
Shaly sand	37.49	39.09	0	154
Sandy shale	9.93	8.35	0	57
Shale	0.11	0.34	0	1.3

Table 4.4 Water saturation of A field

Facies	Water saturation, dec			
	Avg.	Std.	Min	Max
Sandstone	0.51	0.08	0.36	0.73
Shaly sand	0.60	0.11	0.42	0.82
Sandy shale	0.71	0.05	0.49	0.81
Shale	0.72	0.05	0.62	0.82

Table 4.5 Clay volume of A field

Facies	Clay volume, dec			
	Avg.	Std.	Min	Max
Sandstone	4.36	2.01	1	9
Shaly sand	6.38	2.02	1	13
Sandy shale	10.91	6.54	1	30
Shale	24.93	5.98	10	30

Table 4.6 Limestone volume of A field

Facies	Limestone volume, dec			
	Avg.	Std.	Min	Max
Sandstone	0.00	0.00	0.00	0.00
Shaly sand	0.00	0.00	0.00	0.00
Sandy shale	0.00	0.00	0.00	0.00
Shale	0.00	0.00	0.00	0.00

Table 4.7 Correlation coefficient of GR, GRC and GRN

	GR	**GRC**	**GRN**
GR	1.00	0.97	0.76
GRC	0.97	1.00	0.71
GRN	0.76	0.71	1.00

Table 4.8 Correlation coefficient of ILD, ILM and RT

	ILD	**ILM**	**RT**
ILD	1.00	0.89	0.98
ILM	0.89	1.00	0.80
RT	0.98	0.80	1.00

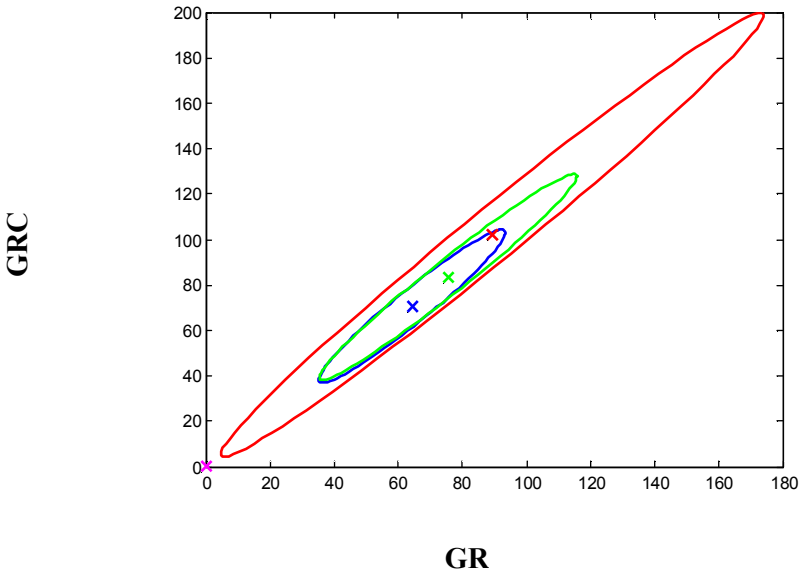

(a) GR vs GRC

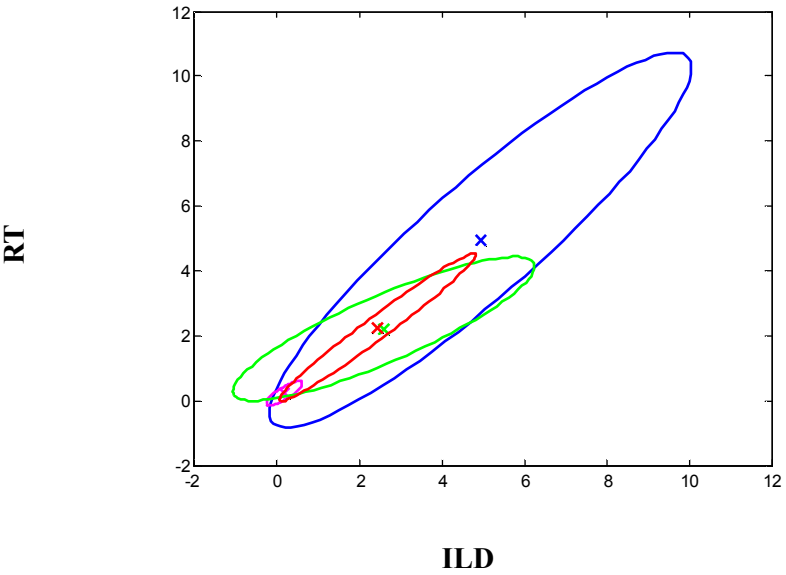

(b) ILD vs RT

Figure 4.1 2D plots of 95% confidence regions for each facies.

4.1.2 Results

Table 4.9 shows the information of HMM parameters such as Π, A and B in order to predict W1 and W2 unknown facies. Π is the global proportions of sandstone, shaly sand, sandy shale and shale. Transition matrix, A, is optimized by EM algorithm. Matrix entries are round off to the nearest hundredths so that 0.00 is not equal to zero and the sum of the row is always l. The output probability, B, is 4 by 30 matrix.

Figure 4.2 illustrates facies profiles at W1. The facies profile is described with four facies such as sandstone (black), shaly sand (dark-gray), sandy shale (gray) and shale (white). Compared to reference, a profile from proposed method mimics better reference than conventional method. Proposed method can remove the meaningless thin layers. **Table 4.10** shows the result by parameters including $C1$ and $C2$. $C1$ and $C2$ are calculated while changing $\Delta\boldsymbol{\rho_{max}}$ as 10, 20 and 40 since it is hard to estimate $\Delta\rho_{max}$ of synthetic field. Owing to the elimination of thin layers, the proposed model shows minor improvement in $C1$ as 2%. On the other hand, in terms of $C2$ which is relevant to the number of facies-transition, the proposed model estimated facies distribution more reliably than conventional method. The reason why thin layers occur in conventional methods is as follows. When various loggings are used simultaneously, facies classification can be vague as shown in **Figure 4.3**. Thin layer can occur in this situation because the conventional method predicts facies only based on most likely probability at depth.

The proposed method and conventional method are applied to W2 where

the facies distribution is thinner than W1. Sand layers contain three thin layers with shaly sand, shale and sandy shale shown as **Figure 4.4**. **Figure 4.4** displays facies profile obtained from two HMM methods. The proposed method can detect thin layers similar with conventional method. Furthermore proposed method gives coarse layers at 10,060-10,063 ft. The conventional method expects thin beds at that depth. This is because using various log type can give different facies information by vague input data. **Figure 4.5** is the well log set at W2.

Table 4.9 HMM parameters for W1 and W2 in A field

Parameters	**Value**
Π	$(0.29 \quad 0.47 \quad 0.17 \quad 0.07)$
A	$\begin{pmatrix} 0.78 & 0.18 & 0.46 & 0.00 \\ 0.01 & 0.86 & 0.10 & 0.03 \\ 0.07 & 0.00 & 0.83 & 0.11 \\ 0.08 & 0.03 & 0.01 & 0.87 \end{pmatrix}$
B	4×30 matrix

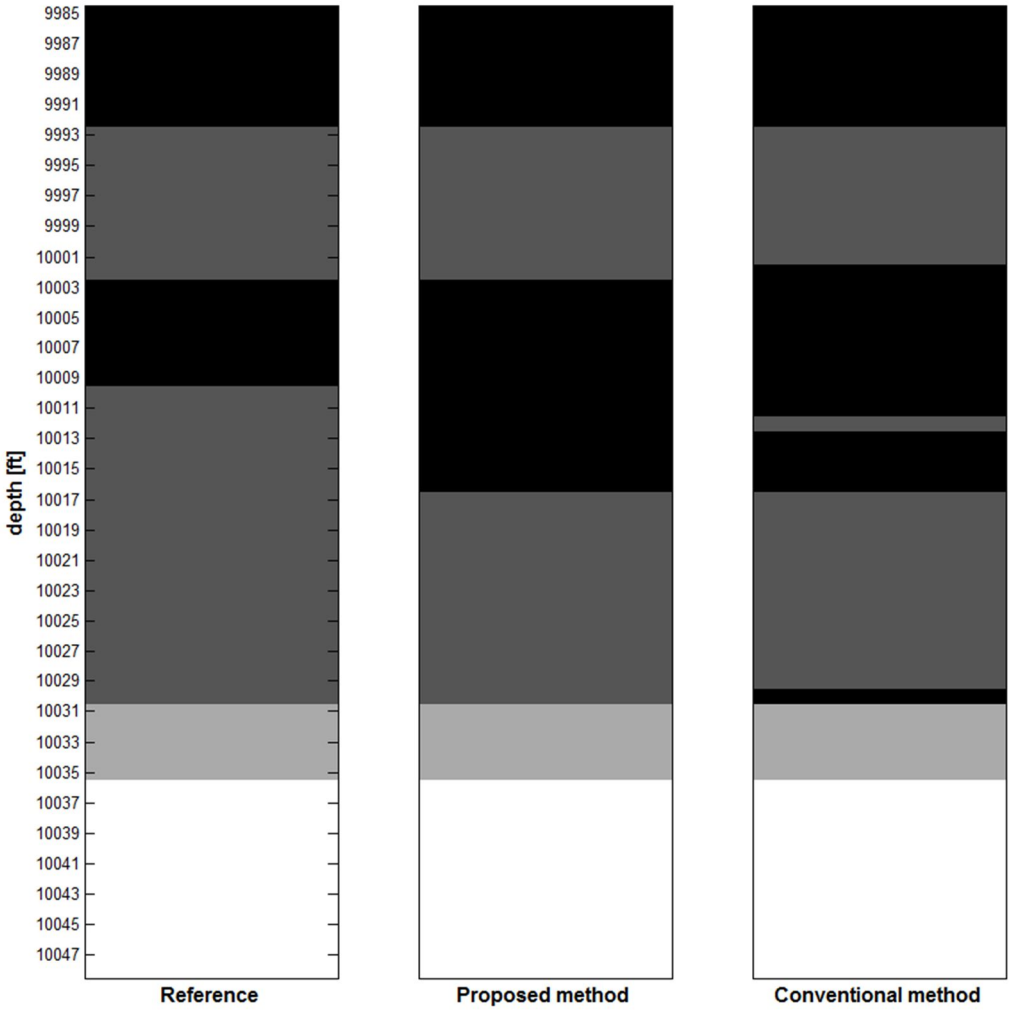

Figure 4.2. Comparison of facies profile at W1 between reference, proposed method and conventional method.

Table 4.10 $C1$ and $C2$ of W1 in A field

		Proposed	Conventional	Difference
	$\boldsymbol{C1}$	0.89	0.88	▲0.02 (▲2%)
	$\boldsymbol{\Delta\rho}$	0	3	▼3
$\boldsymbol{C2}$	$\boldsymbol{\Delta\rho_{max} = 10}$	1.00	0.70	▲0.30 (▲43%)
	$\boldsymbol{\Delta\rho_{max} = 20}$	1.00	0.75	▲0.25 (▲18%)
	$\boldsymbol{\Delta\rho_{max} = 40}$	1.00	0.93	▲0.07 (▲8%)

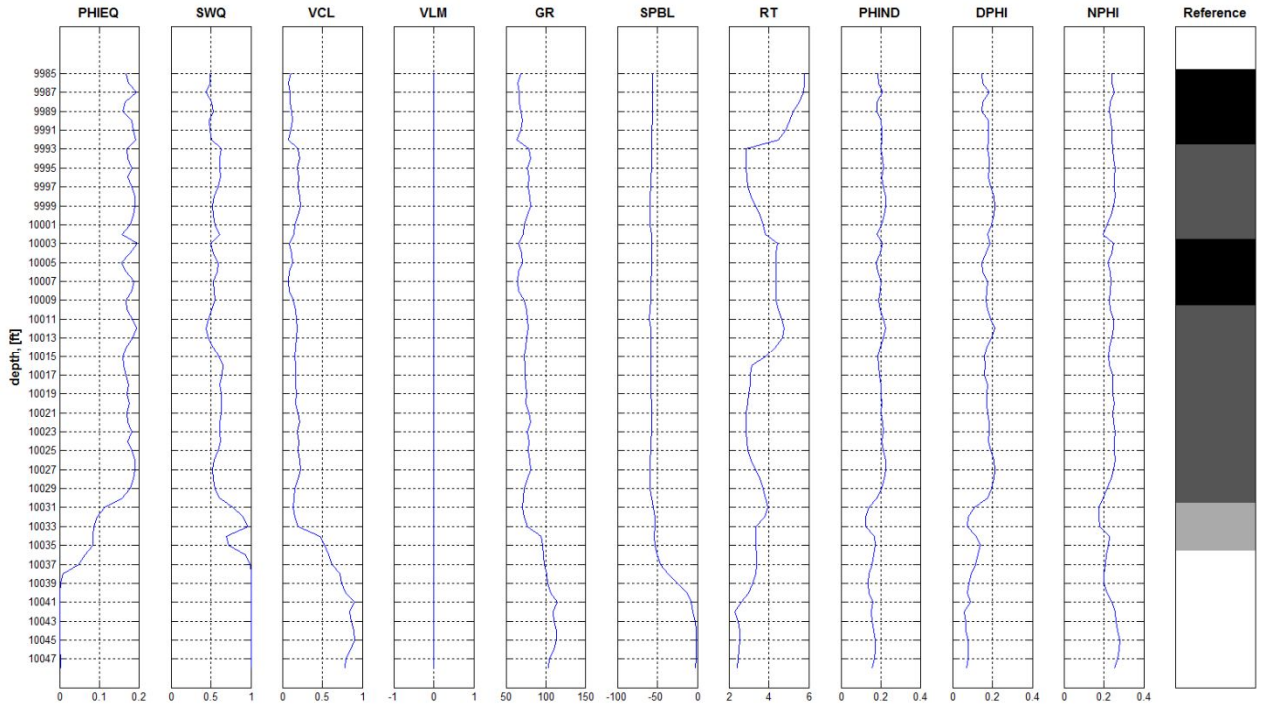

Figure 4.3. Well log set for W1 in A field.

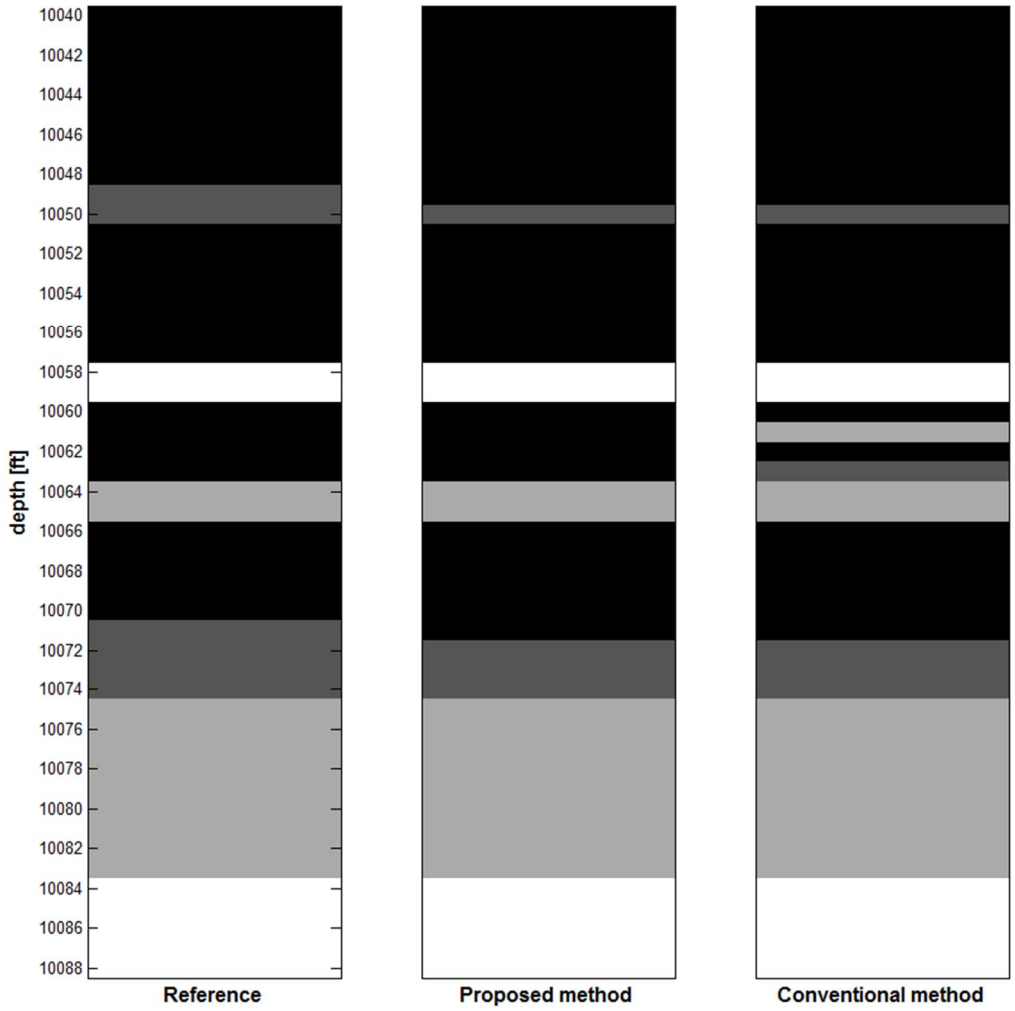

Figure 4.4. Comparison of facies profile at W2 between reference, proposed method and conventional method.

Table 4.11 $C1$ and $C2$ of W2 in A field

		Proposed	Conventional	Difference
	$\boldsymbol{C1}$	0.96	0.92	▲0.04 (▲4%)
	$\boldsymbol{\Delta\rho}$	0	3	▼3
$\boldsymbol{C2}$	$\boldsymbol{\Delta\rho_{max} = 10}$	1	0.70	▲0.30 (▲43%)
	$\boldsymbol{\Delta\rho_{max} = 20}$	1	0.85	▲0.15 (▲18%)
	$\boldsymbol{\Delta\rho_{max} = 40}$	1	0.93	▲0.08 (▲8%)

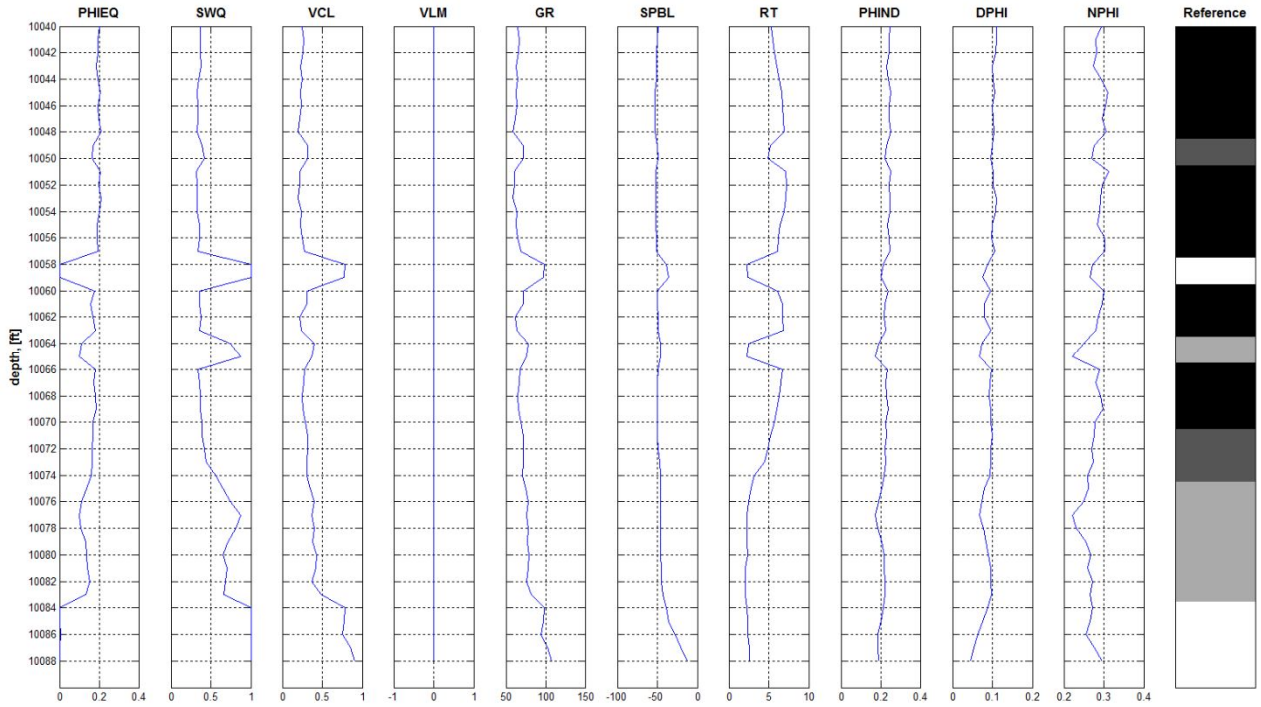

Figure 4.5. Well log set for W2 in Afield.

4.2 Application to synthetic reservoir ‘B’ with five lithofacies

4.2.1 General description

The two HMM methods are applied to synthetic reservoir, B field, which is consist of five different lithofacies such as sandstone, shaly sandstone, sandy sandstone, shale and limestone. **Table 4.12** shows the number of sample for each facies. The dominant facies is sandstone. **Table 4.13, Table 4.14, Table 4.15, Table 4.16 and Table 4.17** represent reservoir properties such as porosity, permeability, clay volume and limestone volume.

GR, SPBL, RT, DPHI, NPHI, PHIND, SWQ, PHIEQ, VCL and VLM are used for input data with 1ft depth interval same as the A field.

Table 4.12 Number of sample in B field

Facies	Sample size	Total
Sandstone	165	
Shaly sand	251	
Sandy shale	156	686
Shale	45	
Limestone	69	

Table 4.13 Porosity of B field

Facies	Porosity, dec			
	Avg.	Std.	Min	Max
Sandstone	0.21	0.02	0.06	0.23
Shaly sand	0.20	0.02	0.05	0.27
Sandy shale	0.18	0.03	0.06	0.23
Shale	0.13	0.05	0.06	0.21
Limestone	0.07	0.06	0.02	0.23

Table 4.14 Permeability of B field

Facies	Permeability, md			
	Avg.	Std.	Min	Max
Sandstone	50.38	39.54	0.00	197
Shaly sand	33.59	34.14	0.00	154
Sandy shale	11.19	16.60	0.00	142
Shale	2.12	6.81	0.00	41
Limestone	5.97	19.23	0.00	95

Table 4.15 Water saturation of B field

Facies	Water saturation, dec			
	Avg.	Std.	Min	Max
Sandstone	0.51	0.08	0.36	0.77
Shaly sand	0.60	0.11	0.42	0.72
Sandy shale	0.71	0.05	0.48	0.82
Shale	0.73	0.04	0.62	0.82
Limestone	0.60	0.14	0.34	0.76

Table 4.16 Clay volume of B field.

Facies	Clay volume, dec			
	Avg.	Std.	Min	Max
Sandstone	0.18	0.06	0.03	0.31
Shaly sand	0.22	0.08	0.08	0.74
Sandy shale	0.35	0.17	0.16	0.91
Shale	0.79	0.15	0.34	0.95
Limestone	0.14	0.10	0.02	0.80

Table 4.17 Limestone volume of B field

Facies	Limestone volume, dec			
	Avg.	Std.	Min	Max
Sandstone	0.00	0.00	0.00	0.00
Shaly sand	0.00	0.00	0.00	0.00
Sandy shale	0.00	0.00	0.00	0.00
Shale	0.00	0.00	0.00	0.00
Limestone	0.14	0.10	0.12	0.79

4.2.2 Results

Table 4.18 shows value of Π, A and matrix size of B for facies classification of W3. As five lithofacies, Π is 1 by 5 matrix. A is 5 by 5 matrix and B is 5 by 8 matrix.

Figure 4.6 and **Table 4.19** are results of blind-test at W3. The reference facies is consist of five facies such as sandstone (black), shaly sand (dark-gray), sandy shale (gray), shale (light-gray) and limestone (white). The limestone layer are embedded between the shaly sand and bottom of the sandy sand. The proposed method expects the shaly sand layers to be coarser than the conventional method. However, both two HMM methods cannot classify limestone layer on the bottom. This problem is result from limitation of HMM method. Since HMM receives the input logs as discrete value, it can detect that the limestone volumes is over 0.18. Also, there are many amount of clay there **(Figure 4.7)**. Both $C1$ and $C2$ are increased 13% and 12% (where, $\Delta\boldsymbol{\rho}_{\boldsymbol{max}}$=20). It shows better prediction performance than conventional method.

Table 4.18 HMM parameters for W3 in B field

Parameters	**Value**
Π	$(0.27 \quad 0.41 \quad 0.25 \quad 0.07 \quad 0.11)$
A	$\begin{pmatrix} 0.79 & 0.07 & 0.00 & 0.00 & 0.14 \\ 0.00 & 0.81 & 0.15 & 0.16 & 0.02 \\ 0.00 & 0.00 & 0.84 & 0.15 & 0.00 \\ 0.03 & 0.67 & 0.05 & 0.86 & 0.00 \\ 0.02 & 0.28 & 0.38 & 0.01 & 0.65 \end{pmatrix}$
B	5×18 matrix

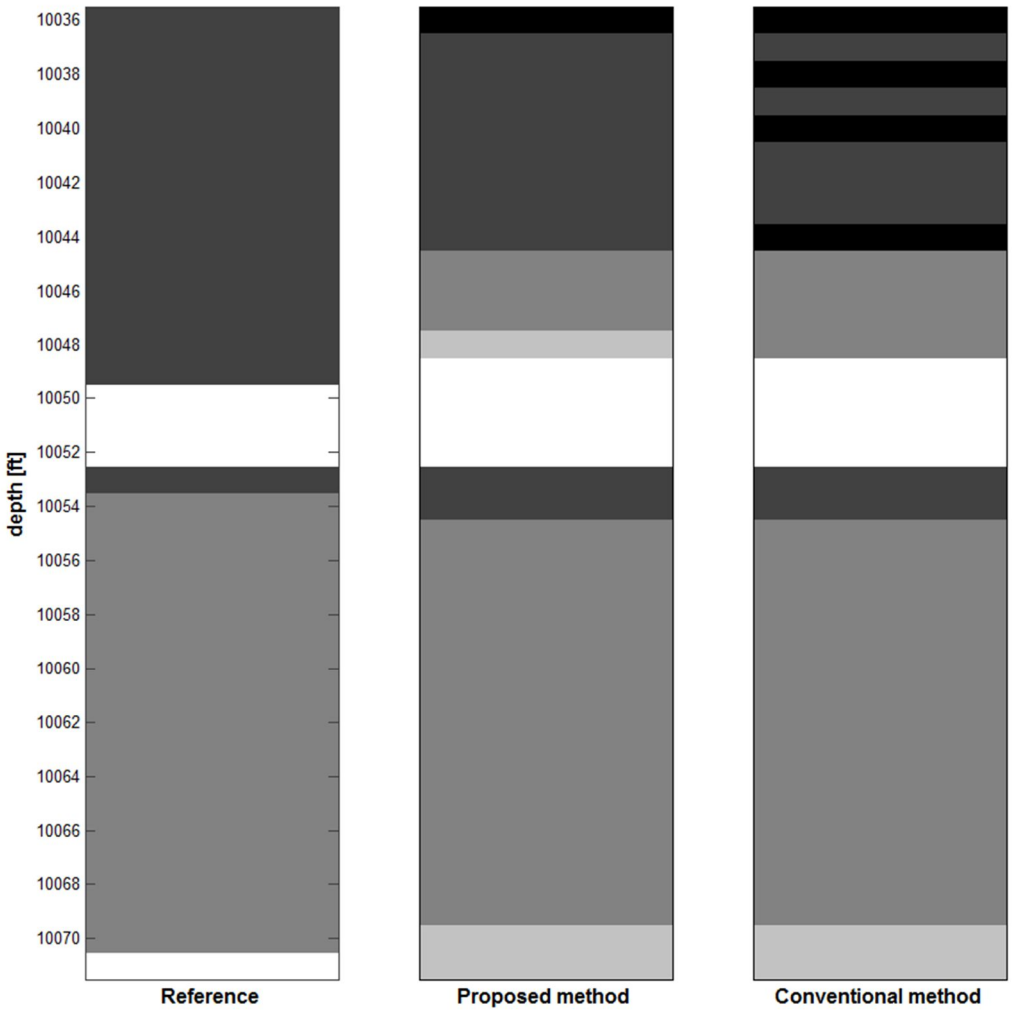

Figure 4.6. Comparison of facies profile at W3 between reference, proposed method and conventional method.

Table 4.19 $C1$ and $C2$ of W3 in B field

		Proposed	Conventional	Difference
	$\boldsymbol{C1}$	0.75	0.67	▲0.08 (▲13%)
	$\boldsymbol{\Delta\rho}$	3	7	▼4
$\boldsymbol{C2}$	$\boldsymbol{\Delta\rho_{max} = 10}$	0.70	0.30	▲0.40 (▲133%)
	$\boldsymbol{\Delta\rho_{max} = 20}$	0.85	0.65	▲0.20 (▲31%)
	$\boldsymbol{\Delta\rho_{max} = 40}$	0.93	0.83	▲0.10 (▲12%)

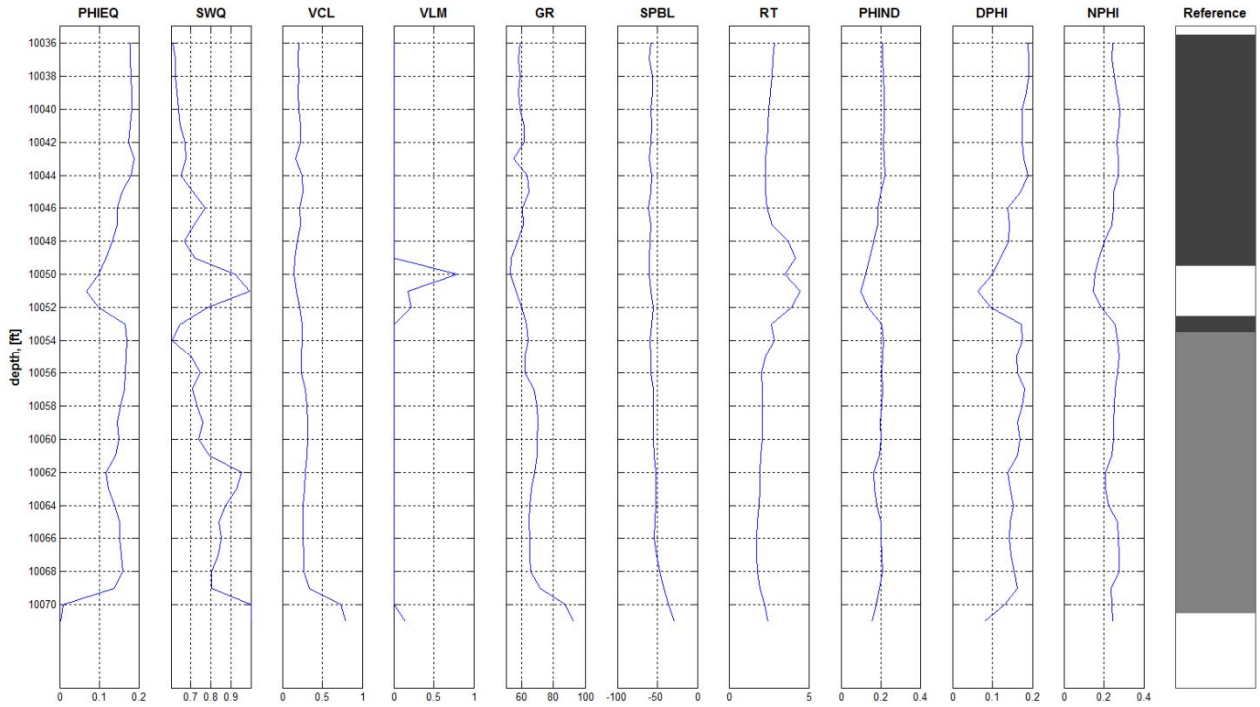

Figure 4.7. Well log set for W3 in B field.

4.3 Application to shoreface reservoir 'C' with four facies

4.3.1 General description

The proposed method is verified on estimating the unknown facies in heterogeneous clastic reservoir. C field is an oil reservoir in Louisiana, USA as shown in **Figure 4.8**. The field is shoreface reservoir which represents at shoreline environment. Since a shoreface facies can be divided into USF, MSF and LSF, hidden states (facies) is four such as USF, MSF, LSF and NSF. The dominant lithofacies is sandstone in addition, there are shale and limestone. There are a lot of production wells and injection wells. The data are gathered from 18 different wells (PRO-03~PRO-28, IDJ-32). **Figure 4.9** represents location of the 17 production wells from the top. We don't have information about location of the injection well, IDJ-32. A depth interval of well log data is 1ft. There are fourteen common well logs in the C field such as GR, GRC, GRN, SPBL, ILD, ILM, RT, DPHI, NPHI, PHIND, SWQ, PHIEQ, VCL and VLM.

Since $C2$ is sensitivity to $\Delta\rho_{max}$, it is important to set suitable $\Delta\rho_{max}$ in field. $\Delta\rho_{max}$ are obtained from using 316 models by changing HMM process and assuming the reversed event only at the blind well (**Figure 4.10)**. **Table 4.20** represents a range of coverable models. $\Delta\rho_{max}$ as 6, 8 and 10 are raised to a unit based on mean, standard deviation and maximum. In this study, $\Delta\rho_{max}$ is 10 to calculate $C2$. **Table 4.21** and **Table 4.23** show the number of sample size and properties in C field.

Figure 4.8 Location of C field in USA.

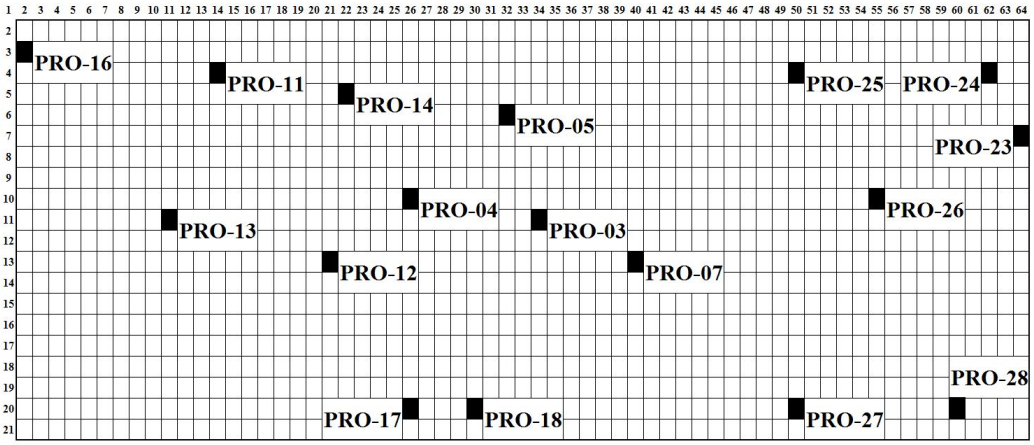

Figure 4.9 Location of 17 production wells in C field.

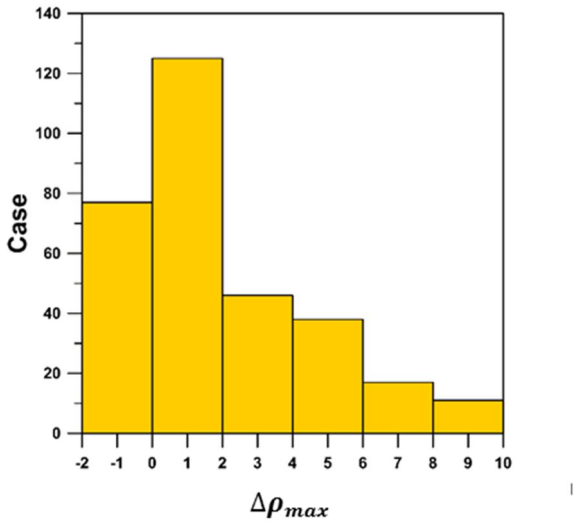

Figure 4.10 Histogram of probable $\Delta\boldsymbol{\rho}$ in C field for 316 models.

Table 4.20 Setting $\Delta\boldsymbol{\rho}_{max}$

$\Delta\boldsymbol{\rho}$	$\Delta\boldsymbol{\rho}_{max}$	**Range**
$\mu + \sigma$	6	91%
$\mu + 1.96\sigma$	8	96%
max	10	100%

Table 4.21 Number of sample in C field

Facies	Sample size	Total
USF	182	669
MSF	278	
LSF	164	
NSF	45	

Table 4.22 Porosity of C field

Facies	Porosity, dec			
	Avg.	Std.	Min	Max
USF	0.20	0.04	0.04	0.23
MSF	0.18	0.06	0.02	0.28
LSF	0.18	0.04	0.04	0.23
NSF	0.13	0.05	0.06	0.21

Table 4.23 Permeability of C field

Facies	Permeability, md			
	Avg.	Std.	Min	Max
USF	47.49	39.95	0	197
MSF	28.67	33.59	0	154
LSF	10.65	16.36	0	142
NSF	2.12	6.81	0	41

Table 4.24 Water saturation of C field

Facies	Water saturation, dec			
	Avg.	Std.	Min	Max
USF	0.53	0.09	0.36	0.77
MSF	0.59	0.11	0.34	0.82
LSF	0.71	0.05	0.48	0.81
NSF	0.73	0.04	0.62	0.82

Table 4.25 Clay volume of C field

Facies	Clay volume, dec			
	Avg.	Std.	Min	Max
USF	0.17	0.06	0.03	0.31
MSF	0.21	0.08	0.02	0.74
LSF	0.34	0.17	0.07	0.91
NSF	0.79	0.15	0.34	0.95

Table 4.26 Limestone volume of C field

Facies	Limestone volume, dec			
	Avg.	Std.	Min	Max
USF	0.01	0.04	0	0.20
MSF	0.02	0.05	0	0.30
LSF	0.01	0.07	0	0.79
NSF	0.00	0.00	0	0.00

4.3.3 Shoreface reservoir

A shoreface is wave-dominated shallow-marine system which is deposited in high or low accommodation space setting **(Figure 4.11)**. Sedimentary structures in shoreface deposits are distinguish with those of laterally equivalent facies. Whereas sediments of the beach and offshore areas are consist of clean sands inhabited by relatively few species of burrowing organisms, the shoreface is characterized by an abundant and diverse fauna inhabiting detritus-rich, muddy sand. Principal sedimentary structures of shoreface deposits are those produced by biogenic reworking, whereas in the laterally equivalent beach and offshore sediments, structures (Reineck et al., 1970; Larue et al., 2005).

Petrophysical properties in shorefaces depositonal environments change gradually due to changes in the coastline. In shoreface environments, the distribution of petrophysical properties is very consistent with parasequence stacking patterns and the opposite occurs for retrogradational stacking patterns. Progradational stacking patterns lead to trends. For example, trend of permeability increasing from base to top (Bueno and Mantilla, 2014).

The USF is excellent quality reservoir sand of shallow marine origin. The USF sands are the dominant lithofacies in the field. These are massive, well-sorted, fine grained sands with extensive original depositional geometries (Kapur et al., 1998).

The LSF is fair-quality reservoir sands of shallow marine origin. These sands are moderate to extensively bioturbated, and their original depositional geometries are extensive (Kapur et al., 1998).

Kapur et al. (1998) studied that the gamma ray log shows the greatest impact for

prediction of USF and MSF in target field. Also, the density log is most important for the prediction of the LSF among four kind of logs including the neutron log and the resistivity log.

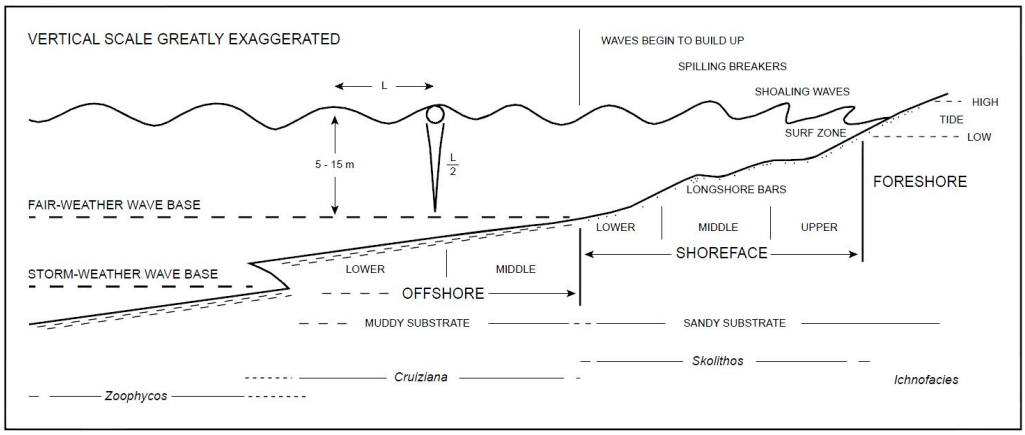

Figure 4.11 Schematic of the shoreline to shallow marine profile (Julianne, 2013).

4.3.3 Results

In order to predict facies distribution for production well, PRO-14, located in relatively middle of the C field, the HMM parameter are set shown as **Table 4.27**. GR, SPBL, RT, DPHI, NPHI, PHIND, SWQ, PHIEQ, VCL and VLM are used for input well logs. **Figure 4.12** and **Table 4.28** show the result of the blind test. The USF, MSF, LSF and NSF are illustrated with different colors such as black, dark-gray, gray and white respectively. As the reservoir properties in shorefaces depositional environments change gradually, it is quite difficult to detect the boundary clearly. Both proposed method and conventional method expect different boundary with reference. The proposed method expects thicker MSF than reference. This is because a lot of well logs significantly change at depth 10,118ft shown as (**Figure 4.13**). The proposed method can mimic the real field. $C1$ and $C2$ were shown as 14% and 400% better prediction performance than conventional method. This is because proposed method can remove the meaningless thin beds by reflecting the facies type of next depth. The proposed method have an opportunity to correct the facies type after one steps.

Table 4.27 HMM parameters for PRO-14 well in C field

Parameters	**Value**
Π	$(0.28 \quad 0.41 \quad 0.24 \quad 0.06)$
A	$\begin{pmatrix} 0.92 & 0.07 & 0.00 & 0.00 \\ 0.05 & 0.83 & 0.12 & 0.00 \\ 0.00 & 0.00 & 0.88 & 0.11 \\ 0.01 & 0.00 & 0.02 & 0.97 \end{pmatrix}$
B	4×30 matrix

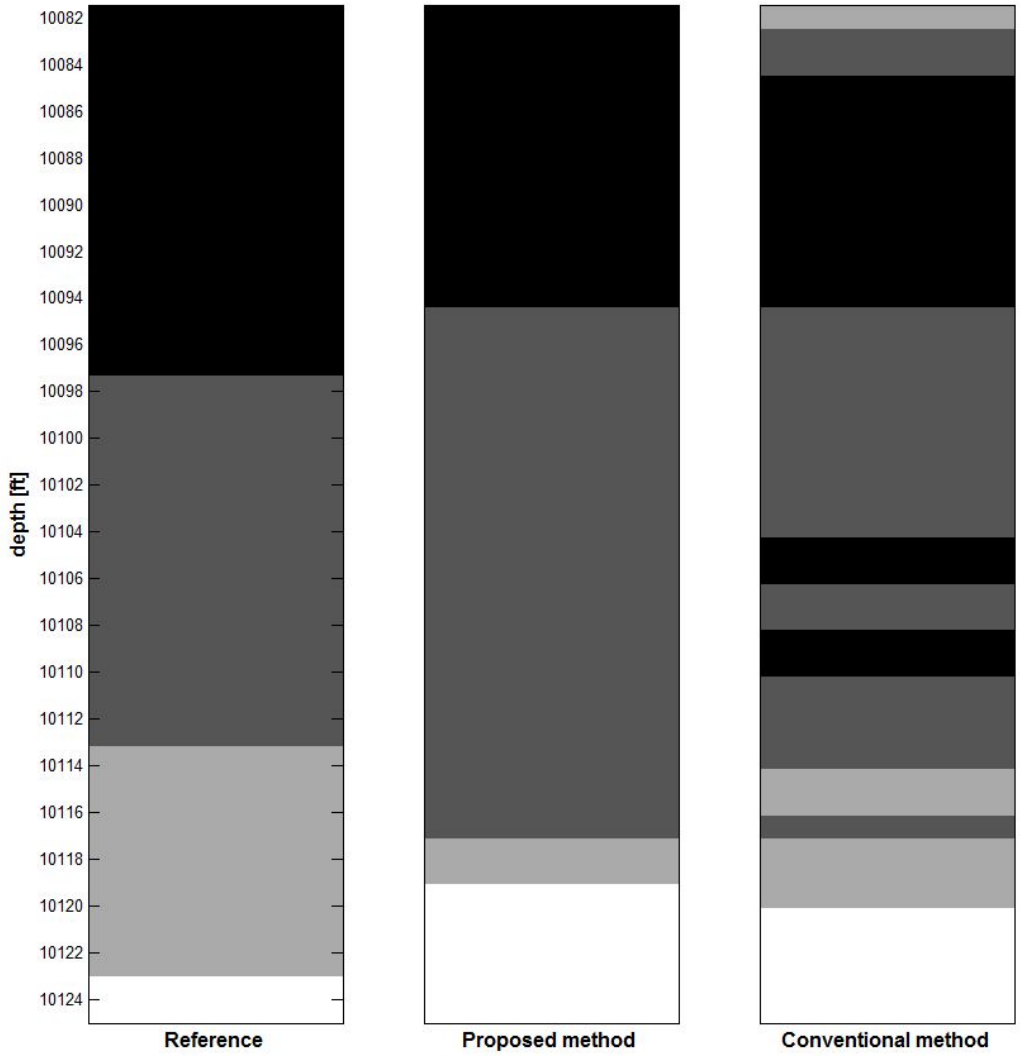

Figure 4.12. Comparison of facies profile at PRO-14 between reference, proposed method and conventional method.

Table 4.28 $C1$ and $C2$ of PRO-14 in C field

	Proposed	**Conventional**	**Difference**
$\boldsymbol{C1}$	0.96	0.84	▲0.11 (▲14%)
$\boldsymbol{C2}$	1.00	0.20	▲0.80 (▲400%)
$\boldsymbol{\Delta\rho}$	0	8	▼8

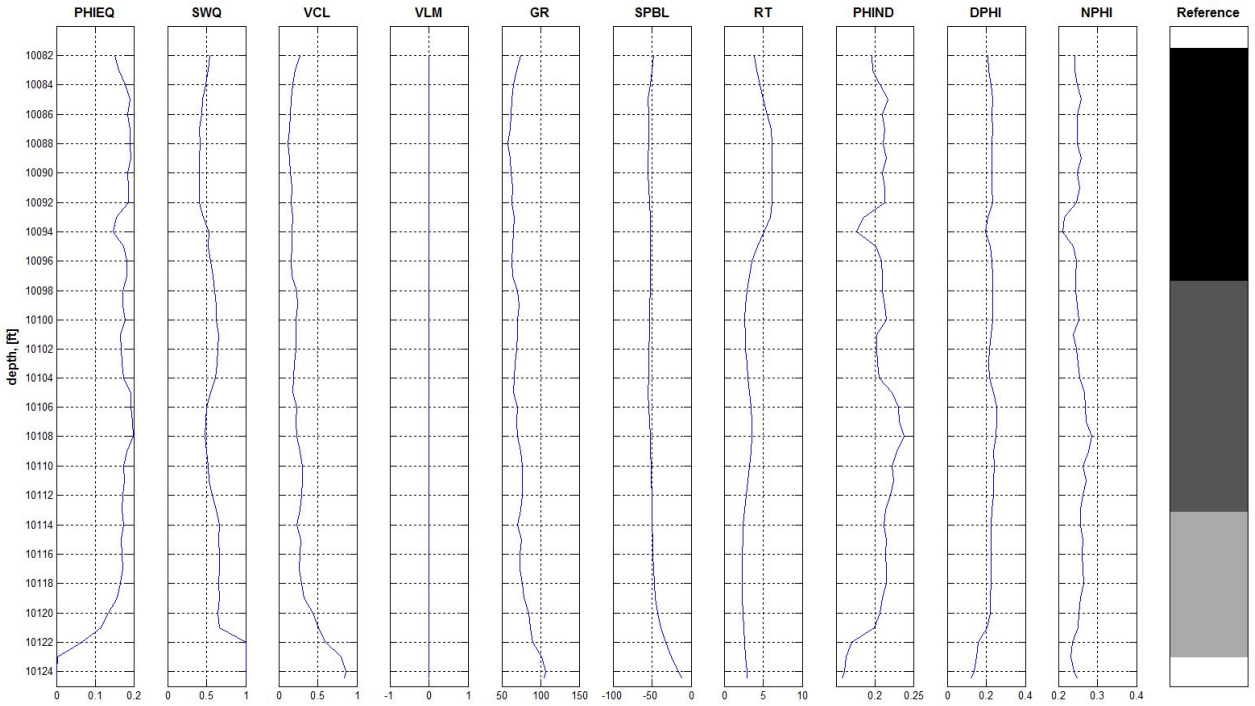

Figure 4.13. Well log set for PRO-14 in C field.

Table 4.29 is the results of the cross validation for 18 wells. Average of $C1$ is 0.79 and $C2$ is 0.94 from the proposed method. Since it decreases difference with reference transition frequency, it gives 12% and 70% higher $C1$ and $C2$ than conventional method using MAP. **Figure 4.14** represents the each prediction ratio of the 18 wells through the $C1$- $C2$ plot. A blue star means the average of the 18 wells. The distributions of 18 wells using the proposed method is relative right and upper side than using the conventional method. **Figure 4.15** compares the prediction performance between the proposed method and the conventional method directly. Distribution of $C1$ relatively parallels to y=x, whereas distribution of $C2$ is left side than y=x. However, both HMM methods fails to predict facies sequence at W13. $C1$ is lower than 0.5. This is because W13 have different tendency with others such as missing LSF.

Table 4.29 Average of $C1$ and $C2$ in C field

	Proposed	**Conventional**	**Difference**
$\boldsymbol{C1}$	0.79	0.70	0.09▲ (▲12%)
$\boldsymbol{C2}$	0.94	0.56	0.39▲ (▲70%)
$\boldsymbol{\Delta\rho}$	0.5	0.45	▼4

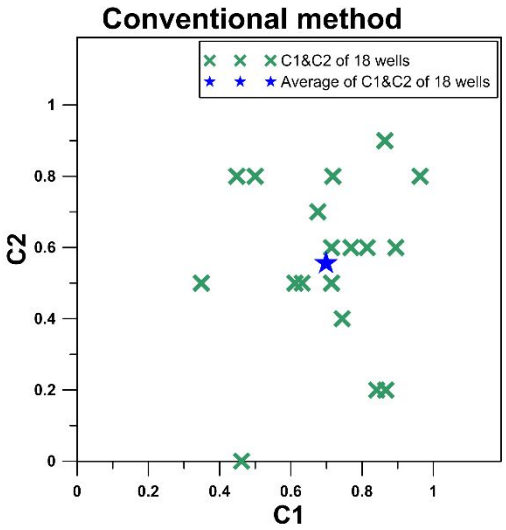

(a)

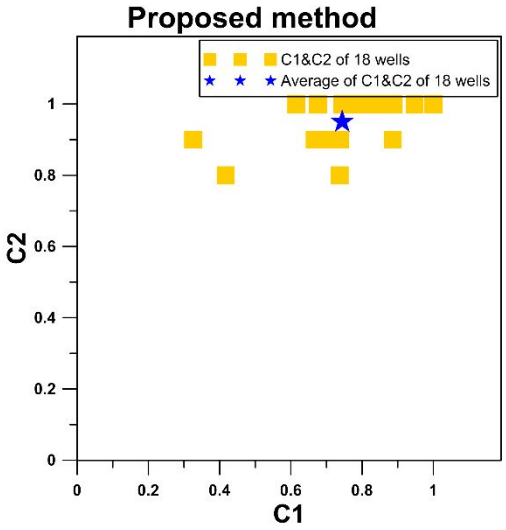

(b)

Figure 4.14 Results from conventional method and proposed method.

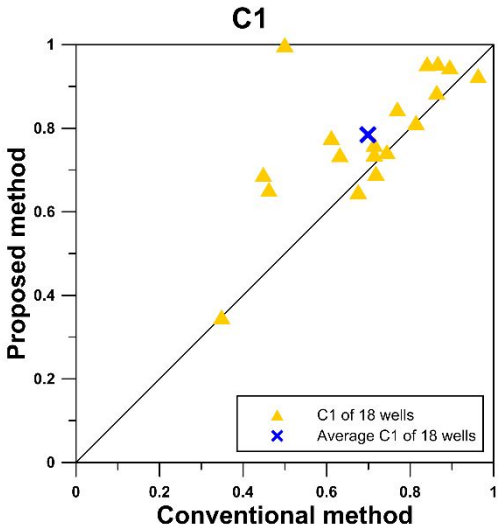

(a)

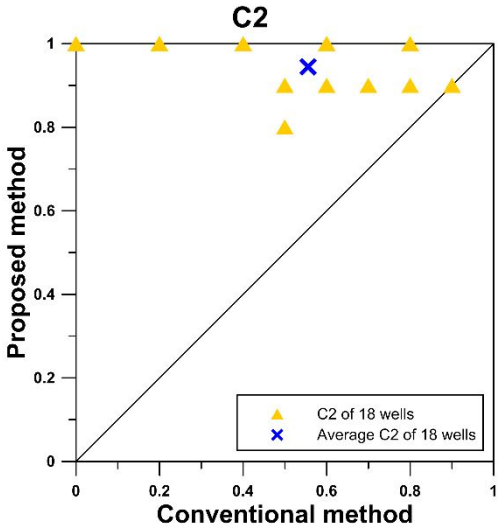

(b)

Figure 4.15 Comparison of $C1$, $C2$ between conventional method and proposed method.

5. Conclusions

In this thesis, a method is proposed to perform facies prediction in clastic reservoir using HMM combined with Viterbi algorithm approach. This approach can minimize noisy effect and is able to select facies sequence close to real facies distributions. The proposed method is applied to three clastic reservoirs, two synthetic reservoirs and shoreface reservoir which is located in the Louisiana, USA. The conclusions of this research work are organized as below.

1. The conventional method fails to match facies because it determines the facies based on MAP. This conventional method provides facies distributions with way too thin layers. This method gives improper results where probabilities are similar or input data is noisy because it cannot reflect the uncertainty of facies determination.

2. On the other hand, the proposed method can mimic realistic facies distributions. The Viterbi algorithm can decrease uncertainty of facies determination because it considers the next depth facies then modifies the facies suitably. This approach can remove meaningless thin layers from noisy data effect and be very useful for 1D directional statistic methods including HMM. For these reasons, the proposed method is possible to improve predictive accuracy; facies–consistence ratio and transition-consistency ratio.

The proposed method shows more reliable facies distributions than the conventional methods. However, disadvantage of method is that it can consider only one step and still be sensitive to prior results at first depth depending on global facies distribution. The proposed method is expected to establish development strategies with reliable characterization.

Reference

엄재홍, 1977, 은닉 마르코프모델을 이용한 정보 추출, 공학석사논문, 서울대학교, 서울.

Bueno, R. and Mantilla, A., 2014, “Distribution of petrophysical properties based on depositional environment: example from fluvial meandering channel and shoreface depositional environments,” SPWLA 55th Annual Logging Symposium, SPWLA, Abu Dhabi, United Arab Emirates, May 18-22.

Baum, L. E. et al., 1970, “A maximization technique occurring in the statistical analysis of probabilistic functions of Markov chains,” The Annals of Mathematical Statistics Vol. 41, No. 3, pp.164–171.

David, F. G. Jr., 1973, “The Viterbi algorithm,” Proceedings of the IEEE Vol. 61, No. 3, pp. 268-278.

Dubois, M. K., Bohling, G. C., and Chakrabarti, S., 2007, “Comparison of four approaches to a rock facies classification problem,” Computers & Geosciences Vol. 33, pp. 599-617.

Elfeki, A. and Dekking, M., 2001, “A Markov chain model for subsurface characterization: theory and applications,” Mathematical Geology Vol. 33, No. 5, pp. 569-589.

Eidsvik, J., Mukerji, T., and Switzer, P., 2004, “Estimation of geological attributes from a well Log: an application of hidden Markov chains,” Mathematical Geology Vol. 36, No. 3, pp. 379-397.

Godfrey, R., Muir, F. and Rocca, F., 1980, “Modeling seismic impedance with Markov chains,” Geophysics Vol. 45, No. 9, pp. 1351-1372.

Jeong, C., Park, C., and Kang, J. M., 2013, “A Fuzzy model integrated with electrofacies characterization for permeability prediction,” Energy Sources Part A Vol. 35, No. 1, pp. 66-76.

Julianne, D., 2013, “Characterization of the lower shoreface to offshore reservoir facies of the Cardium formation in East Pembina, Alberta," MS Thesis, University of Calgary, Alberta.

Krumbein, W. C. and Dacey, M. F., 1969, “Markov chains and embedded Markov chains in geology,” Mathematical Geology Vol.1, No.1, pp. 79-96.

Larue et al., 2005, “Geologic models and flow simulation studies of a shorefaces reservoir: from stratigraphic characterization to history matching,” SEG Technical Program Expanded Abstracts 2005, SEG, pp. 2322-2328.

Lim, J. S., Kang, J. M. and Kim J. W., 1997, “Multivariate statistical analysis for automatic electrofacies determination from well log measurements,” SPE Asia Pacific Oil and Gas Conference and Exhibition, SPE, Kuala Lumpur, April 14-16.

Lim, J. S. and Kim J. W., 2004, “Reservoir porosity and permeability estimation from well logs using fuzzy logic and neural networks,” SPE Asia Pacific Oil and Gas Conference and Exhibition, SPE, Perth, Ortober 18-20.

Lindberg, D. V., Rimstad, E. and Omre, H., 2014, “Identification of facies from multiple well logs accounting for spatial dependencies and convolution effects,” 76th EAGE Conference and Exhibition, EAGE, Amsterdam, Netherlands, June 16-19.

Lindberg, D. V. and Grana, D., 2015, “Petro-elastic log-facies classification using the expectation-maximization algorithm and hidden Markov models,” International Association for Mathematical Geosciences 2015, Springer, Vol. 47, No.6, pp. 719-752.

Lou, H. L., 1995, “Implementing the Viterbi algorithm,” IEEE Signal Processing Magazine Vol.12, No. 5, pp. 42-52.

Rabiner, L. R. and Juang, B. H., 1986, “An introduction to hidden Markov models,” IEEE ASSP Magazine Vol. 3, No. 1, pp. 4-16.

Rabiner, L. R., 1989, “A tutorial on hidden Markov models and selected applications in speech recognition,” Proceedings of the IEEE Vol. 77, No. 2, pp. 257-286.

Sinvhal, A. et al., 1984, “Seismic indicators of stratigraphy,” Geophysics Vol. 49, No. 8, pp. 1196-1212.

Tang, H., Toomey, N. and Meddaugh, W., 2011, “Using an artificial-neural-network method to predict carbonate well log facies successfully,” SPE Reservoir Evaluation & Engineering, February, Vol. 14, No 1, pp. 35-44.

Viterbi, A. J., 1967, “Error bounds for convolutional codes and an asymptotically

optimum decoding algorithm," IEEE Transactions on Information Theory Vol. 13, No. 2, pp. 260–269.

Velzeboer, C. J., 1981, "The theoretical seismic reflection response of sedimentary sequences," Geophysics Vol. 46, No. 6, pp. 843-853.

Wu, C. F. J., 1983, "On the convergence properties of the EM algorithm," The Annals of Statistics, Vol 11, No 1, pp. 95–103.

요약(국문초록)

저류층 암상(facies)은 저류층의 공극률 및 유체투과율 등의 측정에 대단히 중요하다. 암상분석을 위한 코어 직접회수는 높은 비용으로 인해 저류층 전구간에서 할 수 없다. 그리하여 코어 미회수 구간의 암상은 물리검층자료로부터 추계학적 기법으로 예측한다.

수직적 공간 분포를 반영할 수 있는 은닉마르코프모델(hidden Markov model)을 이용한 암상 예측은 해당 깊이에서 각 암상이 존재할 확률론적 방법으로 암상을 결정한다. 그러나 기존에 제시된 방법들은 단순히 확률적 최대값을 갖는 암상을 선택하므로 각 암상의 확률이 비슷한 경우에는 예측률이 떨어진다.

본 연구는 Viterbi 알고리즘과 은닉마르코프모델의 결합으로 암상결정의 불확실성을 감소시켜, 무의미한 천부층 예측을 제거하여 암상 예측률을 제고하는 방법을 제안하였다.

제안한 방법은 쇄설성퇴적암으로 이루어진 두 가지 가상 저류층과 실제 현장 저류층에 적용하였다. 미국 루이지애나 주에 위치한 저류층 내 18개 유정에 교차검증 한 결과, 기존의 방법 대비 약 12% 향상된 암상 예측률을 보였다. 암상전이 빈도 일치도(transition-consistency ratio)의 경우, 기존 방법대비 약 70% 증가하였다.

주요어: 저류층 암상 예측, 물리검층자료, 은닉마르코프모델, 비터비 알고리즘

학 번: 2013-21017